Development of a Simultaneously Frequency- and Time-Resolved Raman-Induced Kerr Effect Probe

Mikhail N. Slipchenko,[†] Benjamin D. Prince, Samuel C. Ducatman,[‡] and Hans U. Stauffer*

Department of Chemistry, Iowa State University, Ames, Iowa 50011-3111

Received: May 14, 2008; Revised Manuscript Received: September 30, 2008

We detail the development of an optical probe technique based on time-resolved Raman-induced Kerr effect polarization spectroscopy (tr-RIKES). This technique, termed fs/ps RIKES, combines an ultrafast pump pulse with a narrowband probe that directly allows spectral resolution of low-frequency (0−600 cm^{-1}) modes typically observable via RIKES. The narrowband probe pulse alleviates the need to scan the time delay between pump and probe pulses to observe molecular coherences, thus making this multiplexed technique a convenient probe for studying low-frequency molecular dynamics. An important distinguishing characteristic of this polarization-sensitive technique arises from the fact that the delay between the impulsive pump pulse and the picosecond-duration probe pulse is optimized to maximize suppression of nonresonant background signal. Model systems, including the rotational spectrum of gas-phase hydrogen and the low-frequency vibrational spectrum of neat bromoform, are used to compare fs/ps RIKES with the conventional time-resolved RIKES technique.

I. Introduction

The successful development of ultrafast laser sources in the past two decades has resulted in a wide range of applications and the development of new time-domain-based spectroscopic techniques.[1,2] One well-established method for the observation of ultrafast dynamics associated with low-frequency (0−600 cm^{-1}) motions is Raman-induced Kerr effect [or optical Kerr effect (OKE)] polarization spectroscopy (RIKES).[3−5] This method has also been applied to the study of pure rotational spectra of gases [often termed Raman-induced polarization spectroscopy (RIPS)] with high resolution and sensitivity[6,7] and can therefore be used as a noninvasive diagnostic of temperature in combustion media[8−10] or for concentration determination in gas mixtures.[11,12] In combination with optical heterodyne detection (OHD-OKE, OHD-RIKES) via the introduction of a local oscillator (LO) field, the optical Kerr effect is a highly sensitive technique that is widely applied to studying low-frequency inter- and intramolecular motions involving pure molecular liquids[1,13−19] and solvated species.[20−22] In addition, the LO provides phase sensitivity, which allows the separation of birefringent and dichroic responses of the samples.

More recently, nonlinear optical techniques have been used as probes to observe the dynamics of impulsively stimulated systems. For example, Scherer et al.[23] and Blank and co-workers[24,25] used polarization response spectroscopy and degenerate four-wave mixing, respectively, to probe the evolution of low-frequency solvent modes following optical excitation of solute species. The time-resolved coherent anti-Stokes Raman scattering (CARS) technique has been used to probe excited-state vibrational coherences following excitation via an ultrafast pump pulse.[26−28] Note that these studies are inherently multidimensional techniques, in which the temporal scan traditionally associated with time-resolved nonlinear optical probes must be carried out for each time delay between the impulsive excitation pulse and the nonlinear optical probe pulse combinations.

Multiplexing techniques, based on the use of combinations of broadband and narrowband pulses within nonlinear optical probes, have recently been implemented to great benefit.[29−32] A major advantage of these techniques arises from the removal of one (temporal) dimension. As such, these multiplexed techniques can be readily applied as probes in which a second dimension, such as time,[33] sample position,[29] temperature, and so on, is varied.

In this work, we demonstrate a multiplexed optical technique, termed fs/ps RIKES, that is based on time-resolved homodyne RIKES but allows direct detection of the frequency-domain RIKES spectrum. This technique is not intended to supplant traditional heterodyned OKE as an optimal technique for detection of low-frequency intra- and intermolecular motion. However, the fs/ps RIKES technique, which combines a broadband (∼80-fs duration) pump pulse with a shaped narrowband (∼1.5-ps duration) probe pulse, eliminates the need to scan a time dimension and perform subsequent Fourier analysis associated with time-resolved RIKES, making it a convenient multiplexed probe for fast detection of low-frequency modes in molecular dynamics studies.

This article is organized as follows: First, a theoretical description of time-resolved RIKES is presented to allow a comparison of the signal obtained in spectrally resolved tr-RIKES experiments to that observed in fs/ps RIKES, followed by a description of the experimental method and optical setup. This is followed by a comparison of fs/ps RIKES to conventional RIKES (i.e., RIPS) in measuring the rotational spectrum of gas-phase H_2; subsequently, we demonstrate the application of fs/ps RIKES in the condensed phase in neat bromoform ($CHBr_3$).

II. Theory

A full theoretical consideration of the off-resonant birefringence observed in time-resolved RIKES experiments can be

* Corresponding author. E-mail: hanss@iastate.edu.
[†] Present address: Purdue University, 206 S. Martin Jischke Dr., West Lafayette, IN 47907-2032.
[‡] Present address: Grinnell College Box 3441, Grinnell, IA 50112.

10.1021/jp804283s CCC: $40.75
Published on Web 12/11/2008

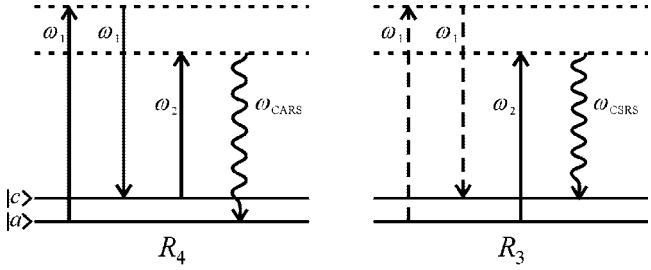

Figure 1. Wave-mixing energy level diagrams for contributing molecular response terms, $R_4(t_3,t_2,t_1)$ (left) and $R_3(t_3,t_2,t_1)$ (right), that survive the rotating-wave approximation for pump (ω_1) and probe (ω_2) pulse carrier frequencies under the conditions described in the text. States $|a\rangle$ and $|c\rangle$ depict, respectively, an initial state and a Raman-accessible state contained within the bandwidth of the pump pulse. Interactions are time ordered from left to right. Solid vertical arrows represent ket-side interactions with the density operator, dashed arrows represent bra-side interactions, and wavy arrows represent the signal field.

found, for example, in Cho et al.[34] and Kinoshita et al.,[35] and Ziegler and co-workers subsequently discussed the nature of spectrally dispersed heterodyne-detected Kerr effect signal.[17,36] In this work, the detected fs/ps RIKES signal and the spectrally dispersed tr-RIKES data presented in section IV contain homodyne-detected signal. As such, expressions are derived for the expected spectrally dispersed homodyne-detected signal under two limiting cases: that of a short broadband probe pulse and that of a narrowband probe.

In the frequency domain, the observed homodyne-detected signal associated with the complex third-order polarization ($P^{(3)}$) is given as a function of signal frequency, ω_s, and pump−probe delay, τ, by[37]

$$S_{\text{homodyne}}(\omega_s,\tau) \propto |P^{(3)}(\omega_s,\tau)|^2 \quad (1)$$

whereas the observed heterodyne-detected birefringence is

$$S_{\text{heterodyne}}(\omega_s,\tau) \propto \text{Im}[\tilde{E}^*_{\text{LO}}(\omega_s)\, P^{(3)}(\omega_s,\tau)] \quad (2)$$

where $\tilde{E}_{\text{LO}}(\omega_s)$ is the frequency-domain local oscillator electric field. Under the rotating-wave approximation (RWA), the resonant contribution to $P^{(3)}$ can be expressed in the time domain as the sum of two surviving time-evolution components[34,37]

$$P^{(3)}(t,\tau) = P^{(3)}_{\text{I}}(t,\tau) + P^{(3)}_{\text{II}}(t,\tau) \quad (3)$$

in which

$$P^{(3)}_{\text{I}}(t,\tau) = \left(\frac{\text{i}}{\hbar}\right)^3 \int_0^\infty \text{d}t_3 \int_0^\infty \text{d}t_2 \int_0^\infty \text{d}t_1 [R_4(t_3,t_2,t_1)\, E_2(t-t_3) \times E_1^*(t+\tau-t_3-t_2)\, E_1(t+\tau-t_3-t_2-t_1) \text{e}^{\text{i}\omega_2 t_3} \text{e}^{\text{i}\omega_1 t_1}] \quad (4)$$

and

$$P^{(3)}_{\text{II}}(t,\tau) = \left(\frac{\text{i}}{\hbar}\right)^3 \int_0^\infty \text{d}t_3 \int_0^\infty \text{d}t_2 \int_0^\infty \text{d}t_1 [R_3(t_3,t_2,t_1)\, E_2(t-t_3) \times E_1(t+\tau-t_3-t_2)\, E_1^*(t+\tau-t_3-t_2-t_1) \text{e}^{\text{i}\omega_2 t_3} \text{e}^{-\text{i}\omega_1 t_1}] \quad (5)$$

and E_1 and E_2 are the electric field envelopes of pulses 1 (pump) and 2 (probe), respectively, temporally separated by delay τ. In these expressions, ω_1 and ω_2 represent the carrier frequencies associated with these respective pulses, R_3 and R_4 are the relevant molecular response functions that survive the RWA, and the carrier frequency, ω_2, associated with this detected polarization has been suppressed.[37] Figure 1 depicts wave-mixing energy level diagrams[38,39] for the R_3 and R_4 contributions to the third-order polarization,[37] which correspond, respectively, to the collinear Stokes and anti-Stokes scattered components of the RIKES signal.[17] Assuming that the electronic dephasing time scales are fast compared to the pulse durations, the variations of pulses 1 and 2 during the electronic coherence times, t_1 and t_3, can be neglected, giving

$$P^{(3)}_{\text{I}}(t,\tau) = \left(\frac{\text{i}}{\hbar}\right)^3 E_2(t) \left[\int_0^\infty \text{d}t_2\, R_4(0,t_2,0)\, |E_1(t+\tau-t_2)|^2\right] \quad (6)$$

An analogous expression for $P^{(3)}_{\text{II}}(t,\tau)$ contains $R_3(0,t_2,0)$ in place of $R_4(0,t_2,0)$. These reduced-dimensionality third-order response functions, R_3 and R_4, can be assumed to take the form

$$R_3(0,t_2,0) = \sum_{a,c} \kappa_{ca} P(a)\, \theta(t_2) \exp(+i\omega_{ca} t_2 - \Gamma_{ca} t_2) \quad (7)$$

and

$$R_4(0,t_2,0) = \sum_{a,c} \kappa_{ca} P(a)\, \theta(t_2) \exp(-i\omega_{ca} t_2 - \Gamma_{ca} t_2) \quad (8)$$

where the summation is carried out over initial states $|a\rangle$ and accessible Raman active states $|c\rangle$; κ_{ca} is a constant containing products of transition dipole moments associated with the nonresonant electronic transitions; $P(a)$ is the population of initial state $|a\rangle$; $\theta(t)$ is a Heaviside step function; and ω_{ca} and Γ_{ca} are, respectively, the Bohr frequency and the dephasing rate associated with the $|c\rangle \leftarrow |a\rangle$ transition.[37] Upon transforming into the frequency domain and focusing first only on the anti-Stokes scattered component, the third-order polarization takes the form

$$P^{(3)}_{\text{I}}(\Delta,\tau) = \frac{1}{\sqrt{2\pi}} \left(\frac{\text{i}}{\hbar}\right)^3 \int_{-\infty}^\infty \text{d}t\, E_2(t) \text{e}^{\text{i}\Delta t} \left[\int_0^\infty \text{d}t_2\, R_4(0,t_2,0) \times |E_1(t+\tau-t_2)|^2\right] \quad (9)$$

where $\Delta = (\omega_s - \omega_2)$ represents the detuning relative to the detected signal carrier frequency, ω_2.

Equation 9 and the analogous expression for $P^{(3)}_{\text{II}}(\Delta,\tau)$ can, of course, be numerically integrated for any forms of pulse 1 and pulse 2 electric fields, and simulated data shown in section IV directly use these expression in combination with eqs 1−3. However, to derive analytical expressions that emphasize the expected signal in two limiting cases—one case involving the use of a short (broadband) probe pulse that is well separated in time and the other involving a narrowband probe pulse—it is instructive to consider additional simplifications of this expression. Assuming that the pulse 1 intensity envelope [$I_1(t) \propto |E_1(t)|^2$] is impulsive compared to the time scales associated with the molecular response during t_2 [i.e., $I_1(t+\tau-t_2) \approx \delta(t+\tau-t_2)$], eqs 7 and 9 can be combined to give

$$P^{(3)}_{\text{I}}(\Delta,\tau) = \frac{1}{\sqrt{2\pi}} \left(\frac{\text{i}}{\hbar}\right)^3 \int_{-\tau}^\infty \text{d}t\, E_2(t) \text{e}^{\text{i}\Delta t} \sum_{a,c} \kappa_{ca} P(a) \times \exp[-i\omega_{ca}(t+\tau) - \Gamma_{ca}(t+\tau)] \quad (10)$$

If the pulse 2 electric field envelope is additionally assumed to have a short [full width at half-maximum (fwhm) = $2(\ln 2)^{1/2}\tau_G$] Gaussian temporal profile, then for pump−probe delays τ that are longer than the pulse 2 duration, the lower integration limit in eq 10 can be set to $-\infty$. Thus, the frequency-domain third-order polarization is

$$P_{\mathrm{I}}^{(3)}(\Delta,\tau) = \left(\frac{\mathrm{i}}{\hbar}\right)^3 \sum_{a,c} \kappa_{ca} P(a) \exp(-i\omega_{ca}\tau - \Gamma_{ca}\tau)\, \tilde{E}_2(\omega_{ca} - \Delta) \exp(\Gamma_{ca}{}^2 \tau_{\mathrm{G}}{}^2/4) \exp\{\mathrm{i}[\Gamma_{ca}(\omega_{ca} - \Delta)\tau_{\mathrm{G}}{}^2/2]\} \quad (11)$$

where $\tilde{E}_2(\Delta)$ is the Gaussian frequency-domain pulse 2 electric field envelope defined by

$$\tilde{E}_2(\Delta) = \frac{1}{\sqrt{2\pi}} \int_{-\infty}^{\infty} E_2(t) \mathrm{e}^{\mathrm{i}\Delta t}\, \mathrm{d}t \quad (12)$$

In contrast, for the case in which pulse 2 has a narrowband spectral profile (as is the case in fs/ps RIKES), the limiting case of a monochromatic (continuous-wave) field 2 can be explored by assuming $E_2(t) = 1$. In this case, eq 10 reduces to

$$P_{\mathrm{I}}^{(3)}(\Delta,\tau) = -\frac{1}{\sqrt{2\pi}} \left(\frac{1}{\hbar}\right)^3 \mathrm{e}^{-\mathrm{i}\Delta\tau} \sum_{a,c} \kappa_{ca} P(a) \frac{1}{(\omega_{ca} - \Delta) - \mathrm{i}\Gamma_{ca}} \quad (13)$$

Application to a Four-Level System (Room-Temperature H_2 Gas). To further explore the homodyne-detected signal observed in these two extreme cases, we use the populated rotational states of room-temperature normal H_2 as a simple four-level system (two pairs of coupled transitions). Assuming that only initial states $|J\rangle$ are populated, where $J = 0$ or 1, and using the $\Delta J = \pm 2$ selection rules for pure Raman transitions in this homonuclear diatomic, eq 11 can be written

$$P_{\mathrm{I}}^{(3)}(\Delta,\tau) = \left(\frac{\mathrm{i}}{\hbar}\right)^3 [C_{20} \exp(-i\omega_{20}\tau - \Gamma_{20}\tau)\tilde{E}_2(\omega_{20} - \Delta) + C_{31} \exp(-i\omega_{31}\tau - \Gamma_{31}\tau)\tilde{E}_2(\omega_{31} - \Delta)] \quad (14)$$

where the coefficients C_{20} and C_{31} collect constants, including transition dipole moments and spin-statistics weighted initial populations, and we have assumed that the dephasing time constants (Γ_{ca}^{-1}) associated with these coherences are long compared to the probe pulse duration, causing the final two exponential arguments in eq 11 to be negligible. In this case, the observed homodyne-detected signal (resulting purely from the $P_{\mathrm{I}}^{(3)}$ term) can be expressed as

$$S_{\mathrm{I,homodyne}}(\Delta,\tau) \propto \left(C_{20}{}^2 \mathrm{e}^{-2\Gamma_{20}\tau} I_2(\omega_{20} - \Delta) + C_{31}{}^2 \mathrm{e}^{-2\Gamma_{31}\tau} I_2(\omega_{31} - \Delta) + 2C_{20}C_{31} \times \exp\left\{ -\left[\frac{(\omega_{31} - \omega_{20})\tau_{\mathrm{G}}}{2} \right]^2 \right\} I_2\{[(\omega_{20} + \omega_{31})/2] - \Delta\} \cos[(\omega_{31} - \omega_{20})\tau] \right) \quad (15)$$

where $I_2(\Delta) = |E_2(\Delta)|^2$ is the pulse 2 spectral distribution (intensity level). The first two terms of this expression therefore represent Gaussian spectral distributions (with bandwidth dictated by the probe pulse spectral width) centered at the Bohr frequencies, ω_{20} and ω_{31}, relative to the pulse 2 carrier frequency, the intensities of which decay with time constants $(2\Gam_{20})^{-1}$ and $(2\Gamma_{31})^{-1}$, respectively. The final term corresponds to oscillations at the difference frequency, $\omega_{31} - \omega_{20}$, over a spectral profile centered at the average Bohr frequency, $^1/_2(\omega_{20} + \omega_{31})$. Note that these observed components are all centered on the blue side of the pulse 2 carrier frequency. In fact, the more general expression for S_{homodyne}, including both $P_{\mathrm{I}}^{(3)}$ and $P_{\mathrm{II}}^{(3)}$ gives rise to oscillations both at difference and sum frequencies of the Raman transition frequencies, ω_{20} and ω_{31}. Furthermore, this expression can be extended to include several Raman active transitions (including the $\Delta J = 0$ Rayleigh transitions); each additional term in eq 14 will give rise to an additional population decay term in eq 15 and coherence terms with corresponding difference frequencies between pairs of Raman active transition frequencies.

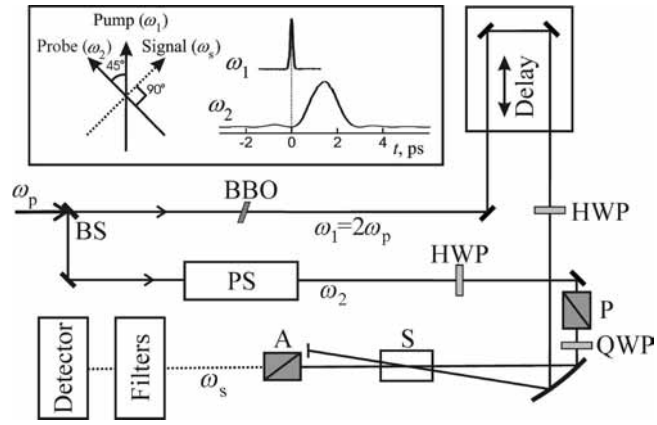

Figure 2. Principal setup for fs/ps RIKES experiments (schematic). Abbreviations used: BS, beam splitter; BBO, frequency doubling crystal; PS, pulse shaper for narrowband filtering of the ω_2 beam; HWP, half-wave plate; QWP, quarter-wave plate; P, polarizer; S, sample; A, analyzer. The inset shows relative polarizations of the beams and the relative timing between pump and probe pulses.

In contrast, in the limit of a long, narrowband pulse 2, the homodyne-detected signal resulting purely from the $P_{\mathrm{I}}^{(3)}$ term is

$$S_{\mathrm{I,homodyne}}(\Delta,\tau) \propto \left(\frac{C_{20}{}^2}{[(\omega_{20} - \Delta)^2 + \Gamma_{20}{}^2]} + \frac{C_{31}{}^2}{[(\omega_{31} - \Delta)^2 + \Gamma_{31}{}^2]} + 2\mathrm{Re}\left\{ \frac{C_{20}C_{31}}{[(\omega_{20} - \Delta) + i\Gamma_{20}][(\omega_{31} - \Delta) - i\Gamma_{31}]} \right\} \right) \quad (16)$$

For transition frequencies, ω_{20} and ω_{31}, that are well separated relative to their respective linewidths [$|\omega_{31} - \omega_{20}| \gg 2(\Gamma_{20} + \Gamma_{31})$], the final cross term can be neglected, and the observed signal is simply a pair of Lorentzian lineshapes centered at the ω_{20} and ω_{31} anti-Stokes-shifted transition frequencies relative to the pulse 2 carrier frequency, with respective linewidths $2\Gamma_{20}$ and $2\Gamma_{31}$ (fwhm). Again, a more general expression for S_{homodyne}, including both $P_{\mathrm{I}}^{(3)}$ and $P_{\mathrm{II}}^{(3)}$ terms, results in additional peaks centered at Stokes-shifted frequencies relative to the pulse 2 carrier frequency. Thus, as is clear from eq 16, the use of a narrowband pulse 2 allows direct observation of the experimental transition frequencies. Despite the inherent homodyne detection necessitated by the use of a narrowband probe pulse in a conventional RIKES experimental setup, no sum or difference frequencies are observed in this narrowband case, as is the case for homodyne-detected signal obtained using conventional RIKES detection schemes.

III. Experimental Setup

The optical system used in these experiments has been described previously.[31] For these particular experiments, the optical layout was modified to allow both conventional tr-RIKES and fs/ps RIKES studies using a standard tr-OKE optical configuration.[40] The relevant aspects of the fs/ps RIKES experimental setup, beam polarization, and timing scheme used are shown schematically in Figure 2. Studies were confined to

the use of two pairs of three beams (experiment-specific details are discussed in section IV): the 795-nm fundamental output (duration: 60 fs, 1 kHz repetition rate) from a Ti:sapphire amplifier (Spectra Physics Spitfire-HPR), the frequency-doubled fundamental beam ($\lambda = 398$ nm, 80 fs), and a tunable visible beam (512 nm, 85 fs; not shown in Figure 2). This visible beam is produced via mixing of the fundamental amplifier output with the infrared signal beam emanating from an optical parametric amplifier (Spectra Physics OPA-800CF) that is pumped by the Ti:sapphire amplifier. For the fs/ps RIKES probe setup, a narrowband probe centered at 795 nm was obtained by directing the broadband 795-nm pulse into a 4*f* pulse-shaping configuration.[41] An adjustable slit (width typically ~250 μm) was placed in the focal plane of this pulse shaper, resulting in a pulse bandwidth of approximately 20 cm^{-1}. This frequency-domain square pulse profile gives rise to a sinc^2 pulse temporal profile, as described previously.[31]

The ω_1 beam polarization is set to 45° relative to the polarization of the ω_2 probe beam using a half-wave plate. The induced birefringence of the sample resulting from interaction with the ω_1 pump pulse is detected by observing the perpendicular component of the ω_2 pulse passing through the analyzer, which is recollimated and focused into a spectrometer (Ocean Optics USB-2000). To compensate for static birefringence from the samples, the relative orientations of the ω_2 pulse polarizer, quarter-wave plate, and analyzer are optimized to maximize the extinction of the ω_2 probe beam prior to measuring OKE-induced birefringence.[3] The achieved extinction of the probe beam was better than 10^6.

In the hydrogen gas-phase experiments, a 40-cm-long room-temperature gas cell, equipped with high-quality 1-mm fused silica windows (CVI), was filled to 2 atm with hydrogen (99.99%). Room-temperature neat bromoform (≥99%, Sigma-Aldrich) studies were carried out using a windowless liquid jet of ~100-μm thickness to eliminate window-induced static birefringence; the jet setup is based on that described by Mathies and co-workers.[42]

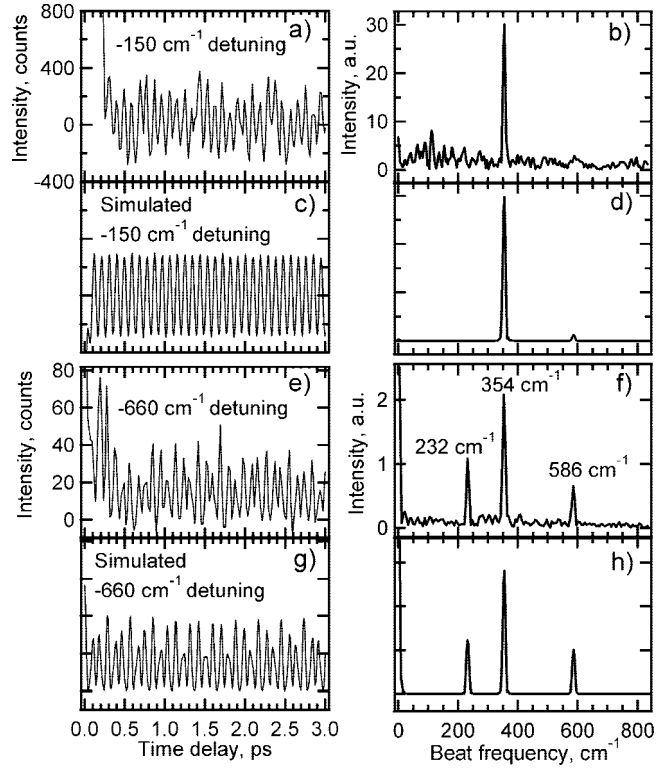

Figure 3. Comparison of experimental and simulated spectrally dispersed tr-RIKES spectra of gas-phase hydrogen at room temperature. Panels a and e show the dispersed (~1-nm resolution) birefringence of hydrogen at two wavelengths detuned from the probe central wavelength (512 nm), after subtraction of the LO background. Panels c and g show the respective simulated data assuming the molecular parameters described in the text. Panels b, d, f, and h show Fourier transform (magnitude) spectra of the 250 fs−6.5 ps time range of the data in panels a, c, e, and g, respectively. These data were obtained in roughly 500 s; a signal-to-noise ratio of roughly 10 was obtained for the most intense observed beat frequencies in the Fourier transform spectra and was limited by laser power fluctuations.

IV. Results and Discussion

A. Gas-Phase Hydrogen Rotational Spectrum. Hydrogen gas was used as a sample for comparison of the traditional tr-RIKES and fs/ps RIKES techniques in the gas phase. In both cases, the pump pulse was the frequency-doubled fundamental centered near 400 nm (20 μJ/pulse). A 512-nm probe (10 μJ/pulse) was used in the heterodyned tr-RIKES studies, based primarily on improved detector sensitivity in this spectral region, whereas a narrowband 800-nm probe (5 μJ/pulse) was used in the fs/ps RIKES technique for optimal spectral resolution dictated by our spectrometer. In the tr-RIKES configuration, the bandwidths of the pump and probe beams are sufficient to excite and probe coherences involving the two lowest Raman-active rotational transitions of hydrogen at 354 and 586 cm^{-1}.[43] Because of static birefringence in the gas cell windows, the intensity of the residual probe beam after extinction was about 10 times larger than that of the signal and served as an LO field in the tr-RIKES experiments. For these experiments, no steps were taken to remove the homodyne contribution to the signal.

In this conventional tr-RIKES configuration, spectral dispersion allows additional selectivity of detected coherences, as the beat frequencies between molecular states have maxima at different detunings from the probe-beam central frequency.[17] Figure 3 shows the spectrally dispersed tr-RIKES signal of hydrogen at two wavelengths: 516 nm (close to the 512-nm maximum of the LO) and 530 nm (where the LO field is negligible) together with the corresponding Fourier transform (FT) magnitude spectra. The experimental data are accompanied by simulated heterodyne and homodyne tr-RIKES signals and their corresponding FT (magnitude) spectra, assuming the four-level system discussed in section II. The simulations were carried out using eq 1 (homodyne) or eq 2 (heterodyne) following numerical determination of $P^{(3)}(\Delta,\tau)$ using eq 9 and an analogous expression for $P_{\mathrm{II}}^{(3)}(\Delta,\tau)$. Pump and probe pulse durations were set to ~70 fs to approximate the experimentally determined pulse durations, and room-temperature Boltzmann statistics (including nuclear spin statistics) were assumed for the initial $J = 0$ and $J = 1$ H_2 state populations. The heterodyne-detected contribution of the $J = 2 \leftarrow J = 0$ beat at 354 cm^{-1} is dominant in the dispersed signal at 516 nm (150 cm^{-1} Stokes detuning from the probe central frequency), whereas contributions of the $J = 3 \leftarrow J = 1$ beat at 586 cm^{-1} together with homodyne signal expected at the beat difference frequency of 232 cm^{-1} are not observed above the noise level. At a larger Stokes detuning of 660 cm^{-1} from the probe central frequency (Figure 3e−h), the contribution from the 354 cm^{-1} beat is much weaker and is comparable in intensity to the contribution of the 586 cm^{-1} beat. Because of the absence of LO field at this detuning, this detected signal results solely from homodyne contributions. Thus, a 232 cm^{-1} beat difference frequency, resulting from cross terms in the squared magnitude of the third-order polarization function (see eq 15), is clearly observed.

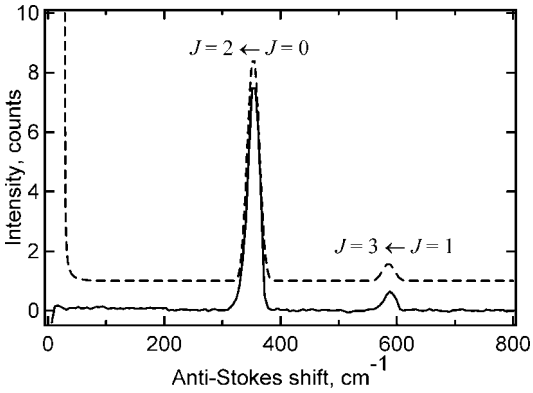

Figure 4. Rotational spectrum of hydrogen gas using the fs/ps RIKES technique (solid curve), after subtraction of background signal from the residual probe beam. The anti-Stokes shift is measured relative to the narrowband probe pulse central frequency. The experimental artifact at zero frequency is a result of subtraction of the intense narrowband probe beam, which was not completely extinguished because of static birefringence in the gas cell windows. A simulation of this spectrum is also shown (dashed curve; see text for details), offset vertically for clarity.

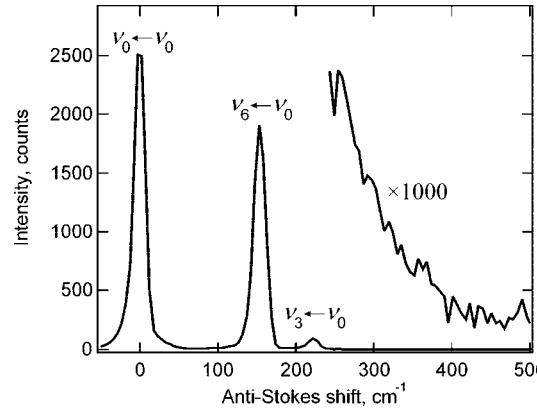

Figure 5. fs/ps RIKES spectrum of $CHBr_3$ taken at a probe pulse delay of 1.4 ps relative to the peak of the pump pulse. The high-frequency region of the spectrum, magnified 1000 times, is also shown in order to emphasize the low noise level and the magnitude of nonresonant signal contributions.

To implement the fs/ps-RIKES setup, a narrowband 795-nm beam was used as a probe. The spectrum of hydrogen obtained using this technique is shown in Figure 4. We note that, for probe pulse delays longer than ~1.0 ps, negligible contributions from a broad nonresonant background were observed in the fs/ps RIKES signal. In the data shown in Figure 4, the peak of the narrowband probe beam was fixed at a 3-ps delay relative to the peak of the ultrafast pump pulse. Two coherences are clearly observed at 354 cm^{-1} ($J = 2 \leftarrow J = 0$) and 586 cm^{-1} ($J = 3 \leftarrow J = 1$) relative to the narrowband probe-beam central frequency, initiating from the two thermally populated states of H_2. The data shown in Figure 4 represent a 300-s data acquisition time, and other than background subtraction of the narrowband ω_2 pulse spectrum, these data are presented as measured. Simulated data included in Figure 4 were calculated using eq 1 following numerical determination of $P^{(3)}(\Delta,\tau)$, as was carried out in the tr-RIKES simulations described above. In this case, the probe pulse was assumed to be the FT of a frequency-domain chirp-free (constant phase) square pulse with 22 cm^{-1} width, and the simulation was carried out at a fixed pump–probe delay, τ, of 1.5 ps. This delay corresponds to a node in the $sinc^2$ probe pulse intensity profile for a 22 cm^{-1} spectral width and represents the time delay at which the nonresonant contribution to the fs/ps RIKES signal is minimized.[31] To match experimental conditions, the simulated fs/ps RIKES spectrum was convoluted with a 14 cm^{-1} (fwhm) Gaussian spectrometer response. The ~20 cm^{-1} widths of the experimentally observed lines are limited by the ω_2 pulse line width and the spectrometer resolution, rather than by the narrow linewidths expected for H_2 gas (eq 16), based on the long-lived coherences shown in Figure 3.

Note that this purely homodyne-detected RIKES signal is essentially background-free outside the narrowband ω_2 pulse spectral window, yet allows direct observation of the Raman-active transitions accessed by this polarization-sensitive fs/ps RIKES technique. In particular, these measurements are not obscured by the presence of sum and difference frequencies between coherences that are observed in conventional homodyne-detected RIKES studies,[11] as shown by comparing eq 15 (broadband probe) to eq 16 (narrowband probe). As is demonstrated in Figure 4, the major limitation of fs/ps RIKES technique is the quality of the narrowband ω_2 pulse extinction, which can obscure signal within the bandwidth of the narrowband ω_2 pulse spectrum.

B. Condensed-Phase Bromoform Vibrational Spectrum. To investigate the performance of the fs/ps RIKES technique in condensed-phase systems, neat bromoform at room temperature was used as a sample. As in the above fs/ps RIKES detection of H_2 gas, a pump pulse centered near 400 nm (10 μJ/pulse) and a narrowband 800-nm probe (5 μJ/pulse) were used, providing optimal spectral resolution. The spectrum of low-frequency vibrational modes of bromoform liquid obtained with the fs/ps RIKES technique is shown in Figure 5, taken at a fixed pump−probe delay of 1.4 ps. Because of a significantly larger contribution of nonresonant signal for this condensed-phase sample relative to that observed in the gas-phase H_2 sample described above, a more precise optimization of this pump−probe delay, such that the pump beam coincided with the first node of the $sinc^2$ temporal profile of the narrowband probe beam,[31] was necessary in this case. A total acquisition time of 50 s was used for the data shown in Figure 5. The observed intramolecular vibrational modes of bromoform at 153 and 222 cm^{-1} are ν_6 (asymmetric C−Br bend) and ν_3 (symmetric C−Br bend), respectively,[44] with measured spectral widths (18 cm^{-1}) that are limited predominantly by the spectrometer resolution. The peak at 0 cm^{-1} contains the $\Delta\nu = 0$ transitions of bromoform, which, in the time domain, is attributed to a slow diffusive reorientation component.[40,45] The signal-to-noise ratio for the 153 cm^{-1} peak is on the order of 10^4 after about 1-min integration time and is limited by the spectrometer. Note that the spectrometer used here is a handheld device with low sensitivity, and large dark current and 2−3 orders of magnitude better signal-to-noise ratio for the same integration time is expected for a scientific-grade spectrometer. Furthermore, because of the optimized delay of 1.4 ps between pump and probe pulses, the remaining background signal shown in the magnified region of Figure 5, which includes nonresonant contributions, is about 1000 times less intense than the 153 cm^{-1} bromoform peak.

The major advantage of fs/ps RIKES over traditional time-resolved Kerr effect polarization spectroscopies is the removal of a time-domain scan and the necessity for subsequent spectral analysis; frequency-domain spectra are directly observed via the fs/ps RIKES scheme. Despite the quadratic dependence of signal on sample concentration owing to homodyne detection, the dynamic range of the fs/ps RIKES technique demonstrated here ensures its applicability to low-concentration samples.

Furthermore, it is expected that introduction of a broadband LO beam at the probe frequency should remove the limitations associated with homodyne detection, including the quadratic dependence of the detected signal on sample density, although such steps were not taken in these experiments.

V. Conclusions

In this work, we demonstrate a multiplexed optical technique based on Raman-induced Kerr effect polarization spectroscopy. This fs/ps RIKES technique alleviates the need to scan the time delay between pump and probe pulses to observe low-frequency molecular coherences, while preserving time-resolution as a probe of Raman-active motions. The technique was applied to both gas-phase hydrogen and liquid bromoform, and in both cases, it showed a large dynamic range and signal-to-noise ratio, while allowing rapid detection of low-frequency Raman-active modes.

Acknowledgment. S.C.D. is grateful for support from the National Science Foundation under Grant CHE0453444. The authors thank S. E. Bradforth and his group for help with jet construction and R. S. Houk for help with materials. Support from Ames Laboratory is also gratefully acknowledged.

References and Notes

(1) Fleming, G. R.; Joo, T.; Cho, M.; Zewail, A. H.; Letokhov, V. S.; Marcus, R. A.; Pollak, E.; Tannor, D. J.; Mukamel, S. *Adv. Chem. Phys.* **1997**, *101*, 141.
(2) Zewail, A. H. *J. Phys. Chem. A* **2000**, *104*, 5660.
(3) Lotshaw, W. T.; McMorrow, D.; Kalpouzos, C.; Kenney-Wallace, G. A. *Chem. Phys. Lett.* **1987**, *136*, 323.
(4) Levenson, M. D. *Introduction to Nonlinear Laser Spectroscopy*; Academic Press: New York, 1982.
(5) Eesley, G. L.; Levenson, M. D.; Tolles, W. M. *IEEE J. Quantum. Elect.* **1978**, *14*, 45.
(6) Morgen, M.; Price, W.; Ludowise, P.; Chen, Y. *J. Chem. Phys.* **1995**, *102*, 8780.
(7) Rouzee, A.; Boudon, V.; Lavorel, B.; Faucher, O.; Raballand, W. *J. Chem. Phys.* **2005**, *123*, 154309.
(8) Lang, T.; Kompa, K. L.; Motzkus, M. *Chem. Phys. Lett.* **1999**, *310*, 65.
(9) Tran, H.; Lavorel, B.; Faucher, O.; Saint-Loup, R.; Joubert, P. *J. Raman Spectrosc.* **2003**, *34*, 994.
(10) Roy, S.; Kinnius, P. J.; Lucht, R. P.; Gord, J. R. *Opt. Commun.* **2008**, *281*, 319.
(11) Lavorel, B.; Faucher, O.; Morgen, M.; Chaux, R. *J. Raman Spectrosc.* **2000**, *31*, 77.
(12) Tran, H.; Lavorel, B.; Faucher, O.; Saint-Loup, R.; Joubert, P. *J. Raman Spectrosc.* **2002**, *33*, 872.
(13) Chang, Y. J.; Castner, E. W. *J. Chem. Phys.* **1993**, *99*, 113.
(14) Ziegler, L. D.; Fan, R.; Desrosiers, A. E.; Scherer, N. F. *J. Chem. Phys.* **1994**, *100*, 1823.
(15) Lotshaw, W. T.; McMorrow, D.; Thantu, N.; Melinger, J. S.; Kitchenham, R. *J. Raman Spectrosc.* **1995**, *26*, 571.
(16) Chang, Y. J.; Castner, E. W. *J. Phys. Chem.* **1996**, *100*, 3330.
(17) Constantine, S.; Zhou, Y.; Morais, J.; Ziegler, L. D. *J. Phys. Chem. A* **1997**, *101*, 5456.
(18) Wiewior, P.; Radzewicz, C. *Opt. Appl.* **2000**, *30*, 103.
(19) Giraud, G.; Gordon, C. M.; Dunkin, I. R.; Wynne, K. *J. Chem. Phys.* **2003**, *119*, 464.
(20) Scherer, N. F.; Ziegler, L. D.; Fleming, G. R. *J. Chem. Phys.* **1992**, *96*, 5544.
(21) Chesnoy, J.; Mokhtari, A. *Phys. Rev. A* **1988**, *38*, 3566.
(22) Hunt, N. T.; Turner, A. R.; Wynne, K. *J. Phys. Chem. B* **2005**, *109*, 19008.
(23) Park, S.; Flanders, B. N.; Shang, X. M.; Westervelt, R. A.; Kim, J.; Scherer, N. F. *J. Chem. Phys.* **2003**, *118*, 3917.
(24) Underwood, D. F.; Blank, D. A. *J. Phys. Chem. A* **2003**, *107*, 956.
(25) Schmidtke, S. J.; Underwood, D. F.; Blank, D. A. *J. Am. Chem. Soc.* **2004**, *126*, 8620.
(26) Siebert, T.; Maksimenka, R.; Materny, A.; Engel, V.; Kiefer, W.; Schmitt, M. *J. Raman Spectrosc.* **2002**, *33*, 844.
(27) Fujiyoshi, S.; Takeuchi, S.; Tahara, T. *J. Phys. Chem. A* **2003**, *107*, 494.
(28) Fujiyoshi, S.; Ishibashi, T.; Onishi, H. *J. Phys. Chem. A* **2004**, *108*, 11165.
(29) Chen, J. X.; Volkmer, A.; Book, L. D.; Xie, X. S. *J. Phys. Chem. B* **2002**, *106*, 8493.
(30) McCamant, D. W.; Kukura, P.; Yoon, S.; Mathies, R. A. *Rev. Sci. Instrum.* **2004**, *75*, 4971.
(31) Prince, B. D.; Chakraborty, A.; Prince, B. M.; Stauffer, H. U. *J. Chem. Phys.* **2006**, *125*, 044502.
(32) Pestov, D.; Murawski, R. K.; Ariunbold, G. O.; Wang, X.; Zhi, M. C.; Sokolov, A. V.; Sautenkov, V. A.; Rostovtsev, Y. V.; Dogariu, A.; Huang, Y.; Scully, M. O. *Science* **2007**, *316*, 265.
(33) McCamant, D. W.; Kukura, P.; Mathies, R. A. *J. Phys. Chem. A* **2003**, *107*, 8208.
(34) Cho, M. H.; Du, M.; Scherer, N. F.; Fleming, G. R.; Mukamel, S. *J. Chem. Phys.* **1993**, *99*, 2410.
(35) Kinoshita, S.; Kai, Y.; Ariyoshi, T.; Shimada, Y. *Int. J. Mod. Phys. B* **1996**, *10*, 1229.
(36) Zhou, Y.; Constantine, S.; Harrel, S.; Ziegler, L. D. *J. Chem. Phys.* **1999**, *110*, 5893.
(37) Mukamel, S. *Principles of Nonlinear Optical Spectroscopy*; Oxford University Press: New York, 1995.
(38) Lee, D.; Albrecht, A. C. Advances in Infrared and Raman Spectroscopy. In *Advances in Infrared and Raman Spectroscopy*; Clark, R. J., Hester, R. E., Eds.; Heyden: London, 1985; Vol. 12, p 179.
(39) Lee, D.; Albrecht, A. C. *Adv. Chem. Phys.* **1993**, *83*, 43.
(40) McMorrow, D.; Lotshaw, W. T.; Kenney-Wallace, G. A. *IEEE J. Quantum Elect.* **1988**, *24*, 443.
(41) Weiner, A. M. *Rev. Sci. Instrum.* **2000**, *71*, 1929.
(42) Tauber, M. J.; Mathies, R. A.; Chen, X. Y.; Bradforth, S. E. *Rev. Sci. Instrum.* **2003**, *74*, 4958.
(43) Huber, K. P.; Herzberg, G. *Molecular Spectra and Molecular Structure. IV Constants of Diatomic Molecules*; Van Nostrand Reinhold Company: New York, 1979; Vol. 1.
(44) Seifert, G.; Zurl, R.; Patzlaff, T.; Graener, H. *J. Chem. Phys.* **2000**, *112*, 6349.
(45) Farrer, R. A.; Loughnane, B. J.; Fourkas, J. T. *J. Phys. Chem. A* **1997**, *101*, 4005.

JP804283S